Variable Eddington Factor Acceleration of Mixed Finite Element/Linear Discontinuous Galerkin Source Iteration

Samuel S. Olivier, Jim E. Morel

Department of Nuclear Engineering
Texas A&M University
College Station, TX 77843

Abstract

Abstract goes here

Keywords

Running Head

Corresponding Author
Jim E. Morel, Phone: (979)845-6072, FAX: (979)845-6075, E-mail: *morel@tamu.edu.*

1 Introduction

The Variable Eddington Factor (VEF) method, also known as Quasi-Diffusion (QD), was one of the first nonlinear methods for accelerating source iterations in S_n calculations []. It is comparable in effectiveness to both linear and nonlinear forms of Diffusion-Synthetic Acceleration (DSA), but it offers much more flexibility than the DSA. Stability can only be guaranteed with DSA if the diffusion equation is differenced in a manner consistent with that of the S_n equations []. Modern S_n codes often use advanced discretization schemes such as discontinuous Galerkin (DG) since classic discretization schemes such as step and diamond are not suitable for radiative transfer calculations in the high-energy density laboratory physics (HEDLP) regime or coupled electron-photon calculations. Diffusion discretizations consistent with the DG S_n discretizations cannot actually be expressed in diffusion form, but rather must be expressed in first-order or P_1 form, and are much more difficult to solve than standard diffusion discretizations. Considerable effort has gone into the development of "partially consistent" diffusion discretizations that yield a stable DSA algorithm with some degree of degraded effectiveness, but such discretizations are also generally difficult to develop. A great advantage of the VEF method is that the drift-diffusion equation that accelerates the S_n source iterations can be discretized in any valid manner without concern for consistency with the S_n discretization. When the VEF drift-diffusion equation is discretized in a way that is "non-consistent," the S_n and VEF drift-diffusion solutions for the scalar flux do not necessarily become identical when the iterative process converges. However, they do become identical in the limit as the spatial mesh is refined, and the difference between the two solutions is proportional to the spatial truncation errors associated with the S_n and drift-diffusion discretizations. In general the order of accuracy of the S_n and VEF drift-diffusion solutions will be the lowest order accuracy of their respective indepen-

dent discretizations. Although the S_n solution obtained with such a "non-consistent" VEF method is not conservative, the VEF drift-diffusion solution is in fact conservative. This is particularly useful in multiphysics calculations where the low-order VEF equation can be coupled to the other physics components rather than the high-order S_n equations. Another advantage of the non-consistent approach is that even if the S_n spatial discretization scheme does not preserve the thick diffusion limit [], that limit will generally be preserved using the VEF method.

The purpose of this paper is to investigate the application of the VEF method with the 1-D S_n equations discretized with the lumped linear-discontinuous method (LLDG) and the drift-diffusion equation discretized using the constant-linear mixed finite-element method (MFEM). To our knowledge, this combination has not been previously investigated. Our motivation for this investigation is that MFEM methods are now being used for high-order hydrodynamics calculations at Lawrence Livermore National Laboratory []. A radiation transport method compatible with MFEM methods is clearly desirable for developing a MFEM radiation-hydrodynamics code. Such a code would combine thermal radiation transport with hydrodynamics. However, MFEM methods are inappropriate for the first-order form of the transport equation, and are problematic even for the even-parity form. []. Thus the use of the VEF method with a DG S_n discretization and a MFEM drift-diffusion discretization suggests itself. Here we define a VEF method that should exhibit second-order accuracy since both the transport and drift-diffusion discretizations are second-order accurate in isolation. In addition, our VEF method should preserve the thick diffusion limit [], which is essential for radiative transfer calculations in the HEDLP regime. We use the lumped rather than the standard LDG discretization because lumping yields a much more robust scheme, and robustness is essential for radiative transfer calculations in the HEDLP

regime. Because this is an initial study, we simplify the investigation by considering only one-group neutron transport rather than the full radiative transfer equations, which include a material temperature equation as well as the radiation transport equation. The vast majority of relevant properties of a VEF method for radiative transfer can be tested with an analogous method for one-group neutron transport. Furthermore, a high-order DG-MFEM VEF method could be of interest for neutronics in addition to radiative transfer calculations. A full investigation for radiative transfer calculations will be carried out in a future study.

The remainder of this paper is organized as follows. First, we describe the VEF method analytically. Then we describe our discretized S_n equations, followed by a description of the discretized VEF drift-diffusion equation. We next give computational results. More specifically, we describe two ways to represent the S_n variable Eddington factor in the MFEM drift-diffusion equation and several ways to construct the S_n scattering source from the drift-diffusion solution for the scalar flux. Each of these options yields a different VEF method. The accuracy of these methods is then compared to that of the standard lumped LDG S_n solution for several test problems, and the iterative convergence rate of these methods is compared to that of the lumped LDG S_n equations with fully-consistent S_2 Synthetic Acceleration (S_2SA). Finally, we give conclusions and recommendations for future work.

2 Variable Eddington Factor Method

2.1 The Algorithm

The steady state, one group, isotropically scattering, fixed source Linear Boltzmann Equation in 1-D slab geometry is:

$$\mu \frac{\partial \psi}{\partial x}(x,\mu) + \Sigma_t(x)\psi(x,\mu) = \frac{\Sigma_s(x)}{2}\int_{-1}^{1}\psi(x,\mu')d\mu' + \frac{Q(x)}{2}\,, \tag{1}$$

where $\mu = \cos\theta$ is the cosine of the angle of flight θ relative to the x–axis, $\Sigma_t(x)$ and $\Sigma_s(x)$ the total and scattering macroscopic cross sections, $Q(x)$ the isotropic fixed-source and $\psi(x,\mu)$ the angular flux. Applying the Discrete Ordinates angular discretization yields the following set of N coupled, ordinary differential equations:

$$\mu_n \frac{\mathrm{d}\psi_n}{\mathrm{d}x}(x) + \Sigma_t(x)\psi_n(x) = \frac{\Sigma_s(x)}{2}\phi(x) + \frac{Q(x)}{2}\,, 1 \le n \le N\,, \tag{2}$$

where $\psi_n(x) = \psi(x,\mu_n)$ is the angular flux in direction μ_n. The scalar flux, $\phi(x)$, is computed using an N-point Gauss quadrature rule such that

$$\phi(x) = \sum_{n=1}^{N} w_n \psi_n(x)\,. \tag{3}$$

The Source Iteration (SI) scheme decouples the system of equations defined by Eq. 2 by lagging the scattering term. In other words,

$$\mu_n \frac{\mathrm{d}\psi_n^{\ell+1}}{\mathrm{d}x}(x) + \Sigma_t(x)\psi_n^{\ell+1}(x) = \frac{\Sigma_s(x)}{2}\phi^{\ell}(x) + \frac{Q(x)}{2}\,, 1 \le n \le N\,, \tag{4}$$

where the superscripts indicate the iteration index. SI is then: solve Eq. 4 for the $\psi_n(x)$, compute the scalar flux using Eq. 3, update the scalar flux on the right side of Eq. 4, and repeat until the scalar flux converges.

The VEF method adds a drift diffusion acceleration step to increase the rate of convergence of SI. The VEF drift diffusion equations are found by taking the first two moments of Eq. 1:

$$\frac{\mathrm{d}}{\mathrm{d}x}J(x) + \Sigma_a(x)\phi(x) = Q(x)\,, \tag{5a}$$

$$\frac{\mathrm{d}}{\mathrm{d}x}\langle\mu^2\rangle(x)\phi(x) + \Sigma_t(x)J(x) = 0\,, \tag{5b}$$

where $J(x) = \int_{-1}^{1} \mu\psi_(x,\mu)\,\mathrm{d}\mu$ is the current and

$$\langle\mu^2\rangle(x) = \frac{\int_{-1}^{1}\mu^2\psi(x,\mu)\,\mathrm{d}\mu}{\int_{-1}^{1}\psi(x,\mu)\,\mathrm{d}\mu} \tag{6}$$

the Eddington factor. By computing the Eddington factor with the S_n angular flux, Eqs. 5a and 5b can be solved directly for the scalar flux. The drift diffusion scalar flux can then be used to update the scattering term on the right side of Eq. 4. The VEF method is:

1. Given the previous estimate for the scalar flux, $\phi^{\ell}(x)$, solve Eq. 4 for $\psi_n^{\ell+1/2}(x)$.

2. Compute $\langle\mu^2\rangle^{\ell+1/2}(x)$ with:

$$\langle\mu^2\rangle^{\ell+1/2}(x) = \frac{\sum_{n=1}^{N}\mu_n^2\psi_n^{\ell+1/2}(x)}{\sum_{n=1}^{N}\psi_n^{\ell+1/2}(x)}\,.$$

3. Solve Eqs. 5a and 5b for $\phi^{\ell+1}(x)$ using $\langle\mu^2\rangle^{\ell+1/2}(x)$.

4. Update the scalar flux estimate on the right side of Eq. 4 with $\phi^{\ell+1}(x)$ and repeat the iteration process until the scalar flux converges.

Acceleration occurs because the angular shape of the angular flux, and thus the Eddington factor, converges much faster than the scalar flux. In addition, the VEF equations model the contributions of all scattering events at once, reducing the dependence on source iterations to introduce scattering information. The solution from the VEF equations is then an approximation for the full flux and not the $\ell - 1$ collided flux as it was without acceleration.

In addition to acceleration, this scheme allows the S_n equations and drift diffusion equations to be solved with arbitrarily different spatial discretization methods. The following sections present the application of the Lumped Linear Discontinuous Galerkin (LLDG) spatial discretization to the S_n equations and the Mixed Finite Element Method (MFEM) to the VEF drift diffusion equations.

2.2 Lumped Linear Discontinuous Galerkin S_n

The LLDG discretization of Eq. 4 is:

$$\mu_n \left(\psi_{n,i}^{\ell+1/2} - \psi_{n,i-1/2}^{\ell+1/2} \right) + \frac{\Sigma_{t,i} h_i}{2} \psi_{n,i,L}^{\ell+1/2} = \frac{\Sigma_{s,i} h_i}{4} \phi_{i,L}^{\ell} + \frac{h_i}{4} Q_{i,L} \,, \tag{7a}$$

$$\mu_n \left(\psi_{n,i+1/2}^{\ell+1/2} - \psi_{n,i}^{\ell+1/2} \right) + \frac{\Sigma_{t,i} h_i}{2} \psi_{n,i,R}^{\ell+1/2} = \frac{\Sigma_{s,i} h_i}{4} \phi_{i,R}^{\ell} + \frac{h_i}{4} Q_{i,R} \,, \tag{7b}$$

where h_i, $\Sigma_{t,i}$, and $\Sigma_{s,i}$ are the cell width, total cross section and scattering cross section in cell i. The i, L and i, R subscripts indicate the the subscripted value is the left or right discontinuous edge value. The cell centered angular flux is the average of the left and right discontinuous edge fluxes:

$$\psi_{n,i}^{\ell+1/2} = \frac{1}{2} \left(\psi_{n,i,L}^{\ell+1/2} + \psi_{n,i,R}^{\ell+1/2} \right) \,, \tag{8}$$

and the cell edged angular fluxes are defined through upwinding:

$$\psi_{n,i-1/2}^{\ell+1/2} = \begin{cases} \psi_{n,i-1,R}^{\ell+1/2}, & \mu_n > 0 \\ \psi_{n,i,L}^{\ell+1/2}, & \mu_n < 0 \end{cases}, \tag{9a}$$

$$\psi_{n,i+1/2}^{\ell+1/2} = \begin{cases} \psi_{n,i,R}^{\ell+1/2}, & \mu_n > 0 \\ \psi_{n,i+1,L}^{\ell+1/2}, & \mu_n < 0 \end{cases}. \tag{9b}$$

Equations 7a, 7b, 8, 9a, and 9b can be combined and rewritten as

$$\begin{bmatrix} \mu_n + \Sigma_{t,i} h_i & \mu_n \\ -\mu_n & \Sigma_{t,i} + \mu_n \end{bmatrix} \begin{bmatrix} \psi_{n,i,L}^{\ell+1/2} \\ \psi_{n,i,R}^{\ell+1/2} \end{bmatrix} = \begin{bmatrix} \frac{\Sigma_{s,i} h_i}{2} \phi_{i,L}^{\ell} + \frac{h_i}{2} Q_{i,L} + 2\mu_n \psi_{n,i-1,R}^{\ell+1/2} \\ \frac{\Sigma_{s,i} h_i}{2} \phi_{i,R}^{\ell} + \frac{h_i}{2} Q_{i,R} \end{bmatrix}, \tag{10}$$

for sweeping from left to right ($\mu_n > 0$) and

$$\begin{bmatrix} -\mu_n + \Sigma_{t,i} h_i & \mu_n \\ -\mu_n & -\mu_n + \Sigma_{t,i} h_i \end{bmatrix} \begin{bmatrix} \psi_{n,i,L}^{\ell+1/2} \\ \psi_{n,i,R}^{\ell+1/2} \end{bmatrix} = \begin{bmatrix} \frac{\Sigma_{s,i} h_i}{2} \phi_{i,L}^{\ell} + \frac{h_i}{2} Q_{i,L} \\ \frac{\Sigma_{s,i} h_i}{2} \phi_{i,R}^{\ell} + \frac{h_i}{2} Q_{i,R} - 2\mu_n \psi_{n,i+1,L}^{\ell+1/2} \end{bmatrix}, \tag{11}$$

for sweeping from right to left ($\mu_n < 0$). The right hand sides of Eqs. 10 and 11 are known as the scalar flux from the previous iteration, the fixed source, and the angular flux entering from the previous cell are all known. By supplying the flux entering the left side of the first cell, the positive-angled solution can be propagated from left to right by solving Eq. 10. Similarly, supplying the incident flux on the right boundary allows the negative-angled solution to be propagated from right to left with Eq. 11.

2.3 Mixed Finite Element Method VEF Drift Diffusion

Applying the MFEM to Eqs. 5a and 5b and enforcing continuity of current yields:

$$-\frac{6}{\Sigma_{t,i}h_i}\langle\mu^2\rangle_{i-1/2}\phi_{i-1/2}+\left(\frac{12}{\Sigma_{t,i}h_i}\langle\mu^2\rangle_i+\Sigma_{a,i}h_i\right)\phi_i-\frac{6}{\Sigma_{t,i}h_i}\langle\mu^2\rangle_{i+1/2}\phi_{i+1/2}=Q_ih_i\,, \quad (12a)$$

$$\begin{aligned}-\frac{2}{\Sigma_{t,i}h_i}\langle\mu^2\rangle_{i-1/2}\phi_{i-1/2}+\frac{6}{\Sigma_{t,i}h_i}\langle\mu^2\rangle_i\phi_i-4\left(\frac{1}{\Sigma_{t,i}h_i}+\frac{1}{\Sigma_{t,i+1}h_{i+1}}\right)\langle\mu^2\rangle_{i+1/2}\phi_{i+1/2}\\ +\frac{6}{\Sigma_{t,i+1}h_{i+1}}\langle\mu^2\rangle_{i+1}\phi_{i+1}-\frac{2}{\Sigma_{t,i+1}h_{i+1}}\langle\mu^2\rangle_{i+3/2}\phi_{i+3/2}=0\,, \quad (12b)\end{aligned}$$

where the Eddington factor is evaluated at iteration $\ell+1/2$ and the scalar flux at $\ell+1$. Here, the Eddington factor has been assumed to be constant in each cell with discontinuous jumps at the edges. The simplest method of converting the Eddington factor from LLDG to MFEM is to compute the Eddington factor using the cell centered and cell edge angular fluxes using Eqs. and 8, 9a, and 9b.

A more consistent way to transfer the Eddington factor is to represent it as a linear function using the MFEM basis functions:

$$\langle\mu^2\rangle_i(x)=\frac{\sum_{n=1}^N\mu_n^2\left[\psi_{n,i,L}B_{i,L}(x)+\psi_{n,i,R}B_{i,R}(x)\right]}{B_{i,L}(x)\sum_{n=1}^N w_n\psi_{n,i,L}+B_{i,R}(x)\sum_{n=1}^N w_n\psi_{n,i,R}} \quad (13)$$

where

$$B_{i,L}(x)=\begin{cases}\frac{x_{i+1/2}-x}{h_i}\,, & x\in[x_{i-1/2},x_{i+1/2}]\\ 0\,, & \text{otherwise}\end{cases} \quad (14)$$

and

$$B_{i,R}(x) = \begin{cases} \frac{x - x_{i-1/2}}{h_i}\,, & x \in [x_{i-1/2}, x_{i+1/2}] \\ 0\,, & \text{otherwise} \end{cases}\,. \tag{15}$$

When MFEM is applied, the integral over cell i of Eq. 13 is approximated with 2 point Gauss quadrature. The cell centered Eddington factors used in Eq. 12 are then:

$$\langle \mu^2 \rangle_i = \frac{1}{2}\left[\langle \mu^2 \rangle_i(x_L) + \langle \mu^2 \rangle_i(x_R)\right] \tag{16}$$

where

$$x_{L/R} = \frac{x_{i+1/2} - x_{i-1/2}}{2} \mp \frac{x_{i+1/2} + x_{i-1/2}}{2\sqrt{3}} \tag{17}$$

are the transformed quadrature points.

Transport consistent boundary conditions are applied through a modified Marshak boundary condition:

$$J(x) = B(x)\phi(x) \tag{18}$$

where

$$B(x) = \frac{\int_{-1}^{1} |\mu| \psi(x,\mu)\,\mathrm{d}\mu}{\int_{-1}^{1} \psi(x,\mu)\,\mathrm{d}\mu}\,. \tag{19}$$

3 Computational Results

The order of accuracy, diffusion limit, and solution convergence were tested in 1D slab geometry with two Eddington factor representations and two scattering term reconstruction methods. The Eddington factor was represented as a piecewise constant with discontinuous jumps at the cell edges and as linear function using the MFEM basis functions. The scattering term reconstruction methods were no reconstruction and maintaining van Leer limited slopes

with the MFEM cell centers. The no reconstruction method set the the left and right discontinuous scalar flux to the MFEM edge scalar flux:

$$\phi_{i,L/R} = \phi_{i\mp 1/2}\,, \tag{20}$$

where the left hand side is the flux used in the LLDG scattering term and the right hand side the MFEM drift diffusion scalar flux. Finally, the van Leer cell centered reconstruction is:

$$\phi_{i,L/R} = \phi_i \mp \frac{1}{4}\xi_{\text{van Leer}}\left[(\phi_{i+1} - \phi_i) + (\phi_i - \phi_{i-1})\right] \tag{21}$$

where $\xi_{\text{van Leer}}$ is the van Leer slope limiter given in []. This reconstruction method is especially important for radiative transfer calculations because the MFEM discretized temperature equation will only have cell centered values.

3.1 Order of Accuracy

The Method of Manufactured Solutions (MMS) was used to compare the accuracy of the VEF method as the cell width was decreased. The L2 norm of the difference between the numerical and MMS solution was compared at five logarithmically spaced cell widths between 0.5 mm and 0.01 mm. A line of best fit of the form

$$E = Ch^n \tag{22}$$

was used to find the order of accuracy, n, and the constant of proportionality, C, of the numerical error, E. These values along with the coefficient of correlation are provided in Table 1 for all six permutations of the two Eddington representation methods and three slope

reconstruction methods. All of the permutations are second order accurate and have similar overall accuracy. This suggests that Eddington representation and slope reconstruction do not affect numerical accuracy. It is also a testament to the robustness of the VEF method as the inconsistent, partially consistent, and fully consistent variations all performed similarly.

Reconstruction Method	Edd. Representation	Order	C	R^2
None	Constant	1.997	0.682	9.9999×10^{-1}
None	Linear	1.998	0.687	1.0000
Center	Constant	2.007	0.726	9.9992×10^{-1}
Center	Linear	2.009	0.732	9.9991×10^{-1}

Table 1: Asymptotic S_4 quadrature for various values of c.

3.2 Diffusion Limit

To test the algorithm in the diffusion limit, the cross sections and fixed source were scaled according to:

$$\Sigma_t(x) \to \Sigma_t(x)/\epsilon\,, \tag{23a}$$

$$\Sigma_s(x) \to \epsilon\Sigma_s(x)\,, \tag{23b}$$

$$Q(x) \to \epsilon Q(x)\,. \tag{23c}$$

In the limit as $\epsilon \to 0$, the system becomes diffusive. Figure 1 shows the number of iterations needed for the VEF method to converge for all six permutations and Fig. 2 shows the L2 norm of the error between the VEF method solution and the exact diffusion solution. These plots show that all of the VEF methods survive the diffusion limit.

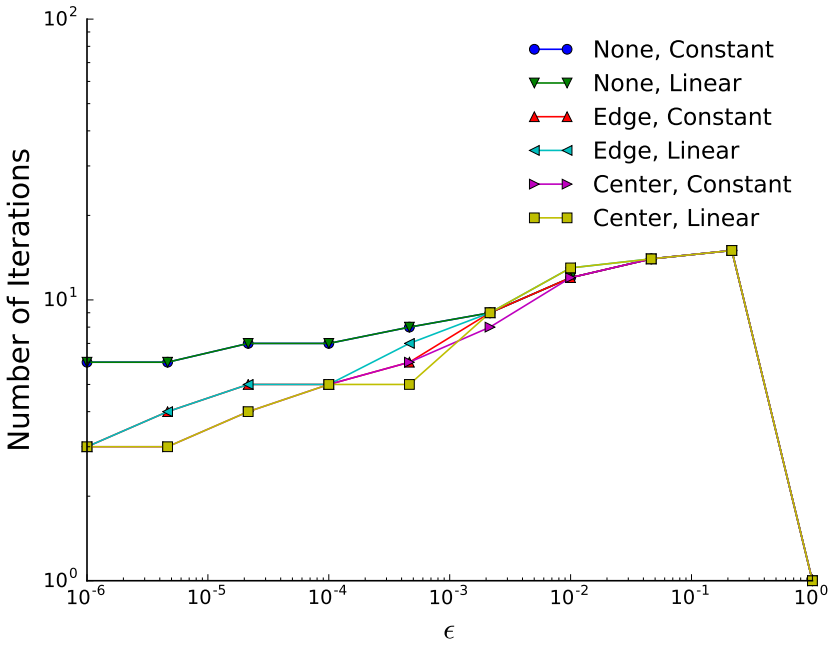

Figure 1: The number of iterations for the VEF method to converge in the limit as $\epsilon \to 0$.

3.3 Solution Convergence

The convergence between unaccelerated SI and the VEF method was compared as a function of cell width for a simple homogeneous slab and for a variant of Reed's problem. In both cases, the slab had a reflecting left boundary and vacuum right boundary. The homogeneous slab had a scattering ratio of 0.75. The cross sections and source for Reed's problem are provided in Table 2. Figure 3 shows the L2 norm of the difference between unaccelerated and VEF accelerated S_8 for the two test problems.

In both cases, the S_n and VEF solutions converge as the cell width is decreased. The convergence for Reed's problem is three orders of magnitudes worse than for the homogeneous slab case. This suggests that

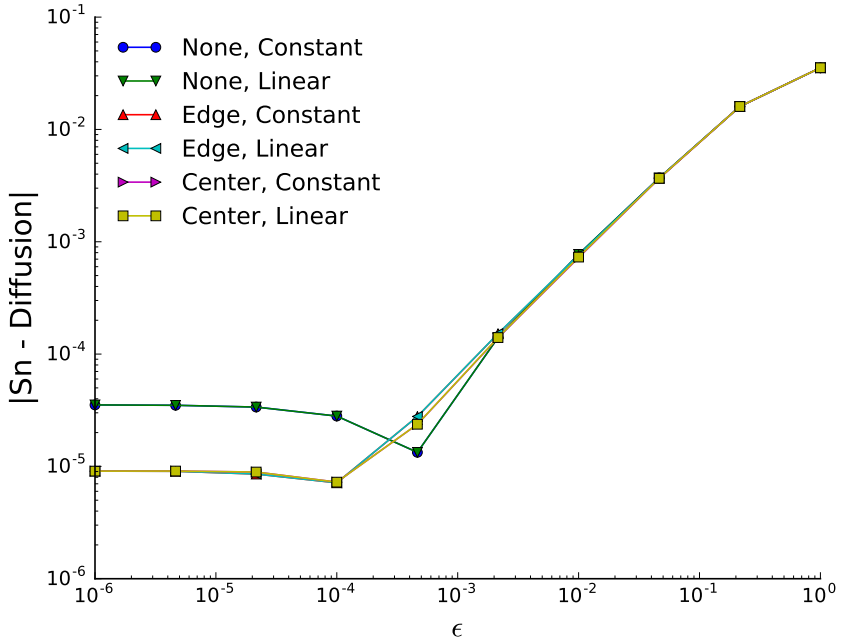

Figure 2: A plot of the error between Diffusion Theory and the VEF solution as $\epsilon \to 0$.

	Region 1	Region 2	Region 3	Region 4	Region 5
q	50	0	0	0	1
Σ_t	50	0.001	1	5	1
Σ_a	50	0	0.1	0	0.1
Domain	$0 \leq x < 2$	$2 \leq x < 4$	$4 \leq x < 6$	$6 \leq x < 7$	$7 \leq x \leq 8$

Table 2: The cross sections and source used for Reed's problem.

3.4 Comparison to S_2SA

4 Conclusions and Future Work

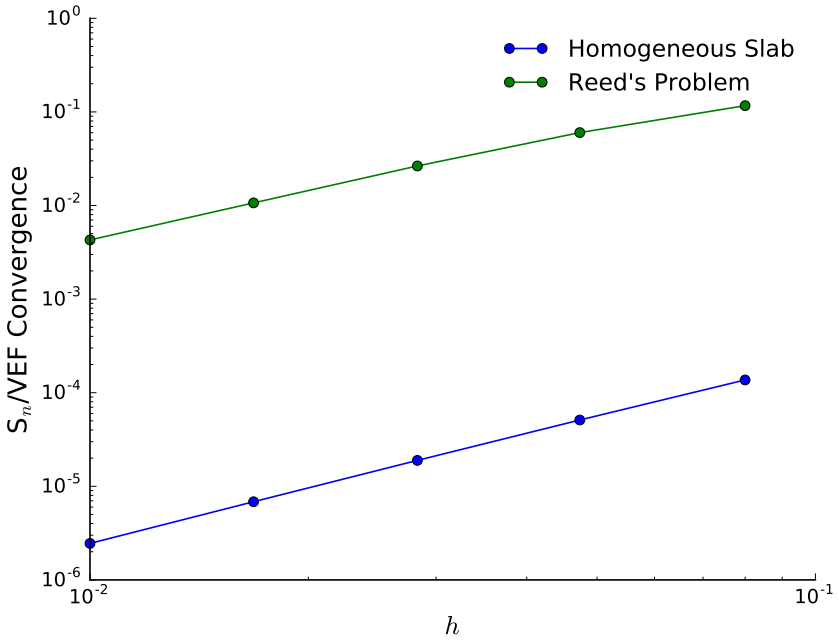

Figure 3: The L2 norm of the difference between unaccelerated and VEF S_8 for a homogeneous slab and Reed's problem.